PHYSICAL REVIEW A VOLUME 14, NUMBER 6 DECEMBER 1976

Temperature dependence of the collisional relaxation processes for the $n = 3$ triplet states of helium

J.-C. Gauthier, F. Devos, and J.-F. Delpech
Groupe d'Electronique dans les Gaz, Institut d'Electronique Fondamentale, Bâtiment 220, Université Paris-XI, Centre d'Orsay, 91405 Orsay, France
(Received 2 August 1976)

Deactivation rates of the $n = 3$ states of the triplet system of helium by collisions with ground-state helium atoms have been measured by time-resolved selective excitation spectroscopy with a short-pulse dye laser as a function of gas temperature from 300 to 600°K. Results are in generally good agreement with predictions of the multistate curve-crossing model for scattering recently proposed by J. S. Cohen; they bring complementary information on the relevant intermolecular potential and on coupling between states.

I. INTRODUCTION

Two inelastic processes may occur in a slow collision between an excited-state and a ground-state helium atom: either nonresonant excitation transfer

$$\mathrm{He}(p) + \mathrm{He}(1\,^1S) \rightarrow \mathrm{He}(q) + \mathrm{He}(1\,^1S)$$

or associative ionization, for large enough excitation energies

$$\mathrm{He}(p) + \mathrm{He}(1\,^1S) \rightarrow \mathrm{He}_2^+(v,K) + e,$$

where p and q represent different quantum states of the atom, and v and K represent a distribution of vibrational and rotational quantum states of the molecular ion.

Significant theoretical advances have been made recently toward an understanding of these processes for states of low principal quantum numbers.[1-3] Using a multistate curve-crossing model for scattering, Cohen[2] has presented averaged cross sections for associative ionization of helium in the n^3S, n^3D, and n^3P states ($n = 3, 4$) and for excitation transfer through ground-state atom collisions from the $n = 3$ state to states with $n = 2$, 3, and 4, for collision energies from thermal to 100 eV.

Extended experimental results were obtained at a neutral temperature around 320 °K by Wellenstein and Robertson.[4] They used a two-step excitation scheme involving first the creation of a relatively large population of singlet [$\mathrm{He}(2\,^1S)$] or triplet [$\mathrm{He}(2\,^3S)$] helium metastable atoms in the positive column of a discharge; the concentration of any $n = 3$ state was then modulated by selective absorption of radiation from a second helium discharge. The transfer rates between levels were finally inferred from the modulation of the concentrations of the other $n = 3$ states, related to the modulations of the corresponding light intensities. Associative ionization rates were deduced from the modulation of the concentration of the molecular helium ion He_2^+ detected with a quadrupole mass spectrometer. A bibliography of earlier theoretical and experimental work will be found in Refs. 1 to 4.

Although Cohen's theory reproduces well the overall features of Wellenstein and Robertson's experiment, several potentially significant discrepancies remain. Furthermore, the relative simplicity of collisional processes originating from the $n = 3$ states makes the temperature dependence of the transfer rates particularly useful and interesting in determining the detailed features of the intermolecular potential curves. It was thus felt necessary to obtain detailed measurements of the effect of neutral temperature changes on the collisional relaxation mechanism of the $n = 3$ states.

Our interest in these topics was also stimulated by the recent development of tuneable pulsed dye lasers and of the associated techniques of time-resolved selective excitation spectroscopy.[5-8]

In the stationary afterglow of a ultrapure helium discharge at pressures of a few Torr, at neutral temperatures ranging from 300 to 600 °K, $\mathrm{He}(2\,^3S)$ metastable concentrations in excess of 10^{11} cm^{-3} are maintained for several hundred microseconds after cessation of the active discharge.[9] We have used a short-pulse dye laser tuned to the 3888.6 Å, $2\,^3S - 3\,^3P$ transition to transfer a small fraction ($\approx 0.5\%$) of the $\mathrm{He}(2\,^3S)$ population to the $\mathrm{He}(3\,^3P)$ level in a few nanoseconds, i.e., in a time short compared to the $\mathrm{He}(3\,^3P)$ lifetime. The steady-state unperturbed populations of the $n = 3$ levels were measured[10] under similar experimental conditions and were found to be of the order of 10^5 cm^{-3}. As a result, the $\mathrm{He}(3\,^3P)$ population is increased by a factor of 10^3 to 10^4 at the end of the laser pulse. Collisional or radiative transitions may then readily transfer the excitation to the neighboring helium states; the relevant part of the triplet term system of helium is shown on Fig. 1. Radiative lifetimes and transfer cross sections

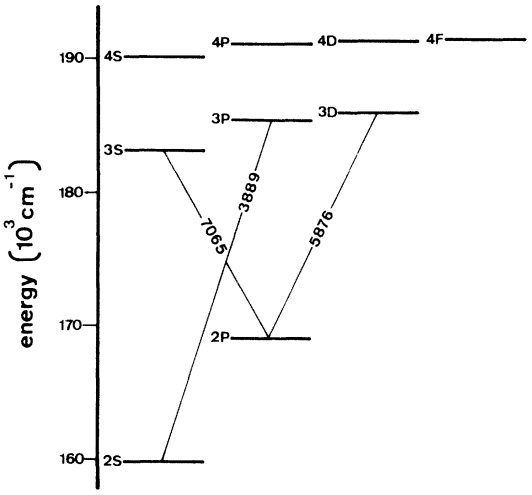

FIG. 1. Term diagram of the relevant triplet states of helium with corresponding transitions (wavelengths in Å).

were deduced from the time-resolved fluorescent emission originating from all the $n = 3$ triplet levels.

II. EXPERIMENTAL SYSTEM

The experimental system is largely similar to the one described in a previous paper on energy relaxation in molecular helium,[7] hereafter referred to as I, as well as in a preliminary report on excitation transfer in atomic helium.[8] Only significant modifications will be reported here.

The high-purity helium cell was made of fused silica; it was centered inside a standard X-band waveguide for microwave diagnostics of afterglow parameters at room temperature. To obtain elevated neutral temperatures, the waveguide was removed and replaced by a small oven with a longitudinal slit for fluorescence light measurements. The wall temperature of the cell was measured with an iron-constantan thermocouple.

Discharge energy is very low and the corresponding heating can be shown to be negligible; in view of the large thermal conductivity of helium, one may fairly assume that gas and wall temperatures are equal; the corresponding systematic error should be negligible.

No impurity lines were observed after prolonged bakeout of the cell and cataphoretic cleaning of the gas, even when the cell was heated to the highest obtainable temperature (600 °K).

At room temperature, electron density and temperature were routinely measured by microwave diagnostics[9] as a function of time in the afterglow. As usual, the electron temperature could be changed at a selected time by a medium-power ($\lesssim 1$ W) pulsed microwave heating field at X-band frequencies around 9 GHz. This was found particularly useful for distinguishing between electron- and neutral-induced excitation transfer. It was possible to raise the average electron energy to a sufficiently high value for ambipolar diffusion (which is linearly proportional to electron temperature) to become the dominant loss term during the heating pulse, while still keeping inelastic electron-metastable collisions to a negligible level.[11] As a result, the electrons could be swept out of the afterglow cell and their influence on excitation transfer could be suppressed, while the other parameters remained unchanged.

The excitation wavelength at 3888.6 Å was obtained from a nitrogen-pumped dye laser[12] which operated with a xylene solution of an equal volume mixture of 2, 5-Di-(4-biphenylyl)-1, 3, 4-oxadiazole (BBD) and 4, 4‴-*bis*-(2-butyloctyloxy)-p-quaterphenyl (BIBUQ). It delivers a typical pulse power of 2 kW in a 3.5-nsec (full width at half maximum) pulse. The spectral width at half maximum was of the order of less than 0.1 Å as measured with a plane Fabry-Perot interferometer.

The fluorescence light observation system was the same as in I. The resolution of the monochromator was set to 2 Å and light intensities were measured with a Hamamatsu R446UR photomultiplier tube (PM) followed by a wide-band, impedance-matching amplifier having an integration time constant of about 6 nsec. The monochromator-PM combination was calibrated for absolute intensity measurements with a tungsten-ribbon filament lamp, itself calibrated by the Bureau National de Métrologie, Paris. The nearly constant sensitivity of the PM over the observed spectral range was particularly appropriate to this experiment. Its linearity range under transient conditions was ascertained by illuminating the photosensitive surface with the laser light after variable, calibrated attenuations; fluorescence light intensities were then kept well below saturation level.

The shape of the fluorescence decay curves was also monitored as a function of laser power over a 1 to 20 range. No saturation of the pumped transition was detected; fluorescence decay time was independent of laser power on all observed transitions and fluorescence intensities were linearly proportional to laser power over the range covered.

An auxiliary, low-resolution monochromator was used to record the maximum fluorescence light intensity on the $3\,^3P$-$2\,^3S$ transition. This intensity was proportional under constant experimental conditions to the laser power available on the width of the line; it was used for normalization of the fluorescence signals and for constant monitoring of

the laser output power.

The laser output beam was linearly polarized (~60%) in the vertical plane, parallel to the grooves of the grating. Polarization of fluorescence may in some cases[13] constitute a significant source of systematic errors in fluorescence intensity and decay measurements. The results reported here are independent of the direction of polarization of the pumping light; fluorescence light on all observed transitions was unpolarized.

The data collection system has been described in I. The output of the multichannel analyzer was punched on paper tape for off-line processing by a computer. The delta-function response of the PM-amplifier combination is identical to its single-photon response, which is easily measured. It was used to deconvolute the data to compensate for the finite integration time constant of the photon detection system; it was thus possible to optimize simultaneously the pulse response and the signal-to-noise ratio of the measuring system. The interval τ between samples was calibrated against a precision pulse generator and the corresponding systematic error was easily made negligible. Figure 2 shows typical deconvoluted results for the evolution of the absolute populations of the three $n=3$ triplet levels during and after selective optical pumping of the $3\,^3P$ level.

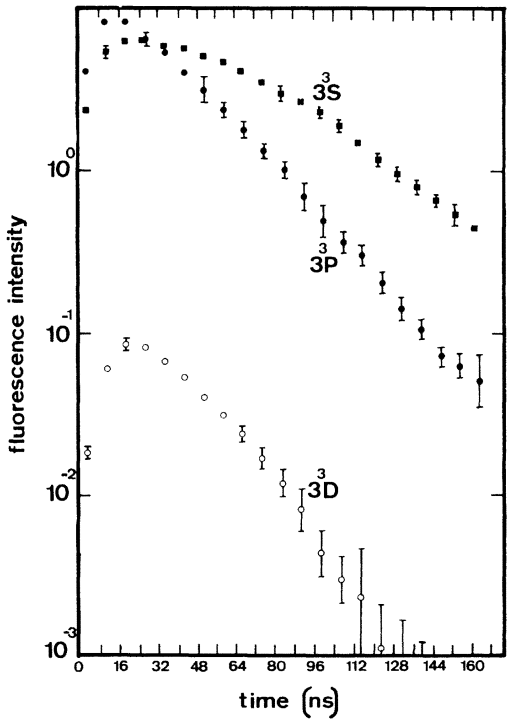

FIG. 2. Fluorescence light intensity in arbitrary units as a function of time. Experimental conditions [He] = 4.6 $\times 10^{17}$ cm^{-3}, $T_g = 300$ °K, [e] = 2.9×10^{11} cm^{-3}, $T_e = 600$ °K. Statistical error bars are representative of data reproducibility.

III. THEORY OF THE EXPERIMENT

The rate equations for the population of the three $n=3$ triplet levels with a laser pumping term $L(t)$ on the He($2\,^3S$) to He($3\,^3P$) transition at 3888.6 Å may be written at time t:

$$\frac{dn_s}{dt}(t) = A_{ss}n_s(t) + A_{ps}n_p(t) + A_{ds}n_d(t), \tag{1a}$$

$$\frac{dn_p}{dt}(t) = A_{sp}n_s(t) + A_{pp}n_p(t) + A_{dp}n_d(t) + L(t), \tag{1b}$$

$$\frac{dn_d}{dt}(t) = A_{sd}n_s(t) + A_{pd}n_p(t) + A_{dd}n_d(t). \tag{1c}$$

The labels s, p, and d correspond to the He($3\,^3S$), He($3\,^3P$), and He($3\,^3D$) levels, respectively. The rate coefficients A_{lm} have a simple physical interpretation: diagonal elements (i.e., where $l=m$) are the total deexcitation rates per unit time of level l (these loss terms are negative) while off-diagonal elements ($l \neq m$) are the l to m transfer rates (these transfer terms are positive).

The experimental system yields as raw experimental data the absolute populations $n_l(t_i)$ of each level at N predetermined times $t_i = i\tau$ for i varying from 1 to N after the beginning of the laser pumping pulse (see Fig. 2); the time interval τ between consecutive data points was 4 or 8 ns, depending on experimental conditions. The derivatives $(dn_l/dt)(t)$ are easily deduced from these data, provided τ is short enough for second-order terms to be negligible. The source term $L(t)$ is deduced directly from the shape of the laser pulse.

After substitution of the measured population densities and of their derivatives at a given time, the system of coupled differential Eqs. (1) reduces to a set of three independent linear equations, each with three rate coefficients as unknown. To be specific, let us focus the discussion on Eq. (1a): after substitution of the measured values of $(dn_s/dt)(t_i)$, $n_s(t_i)$, $n_p(t_i)$, and $n_d(t_i)$ obtained under given experimental conditions at the N times t_i after the beginning of the laser pulse, we obtain a set of N linear equations with the three unknowns A_{ss}, A_{ps}, and A_{ds}; provided, as is always the case, that $N > 3$, this is easily solved by a least-squares method yielding the "best" values of A_{ss}, A_{ps}, and A_{ds} and the corresponding estimates of the statistical error bars.

In fact, it turns out that four of the rate coefficients appearing in Eqs. (1a), (1b), and (1c) cannot be determined significantly within our range of experimental conditions: the first two are A_{sp}

in Eq. (1b) and A_{sd} in Eq. (1c), because the energy difference between the He($3\,^3S$) and He($3\,^3P$) or ($3\,^3D$) levels (2328 or 2865 cm^{-1}) is considerably larger than the average thermal energy (210 to 420 cm^{-1}), leading to a small Boltzmann factor in the excitation rate; the other two factors that cannot be significantly determined are A_{ds} in Eq. (1a) and A_{dp} in Eq. (1b), because the population of level He($3\,^3D$) is always considerably smaller than the populations of the other two levels (see Fig. 2).

As a consequence, the least-squares resolution of Eqs. (1) with the full set of coefficients as described above yields always error bars which are comparable or larger than the coefficient itself for these particular four coefficients. This introduces additional statistical fluctuations on the five remaining coefficients, and it is desirable to use as much *a priori* information as possible to reduce the number of degrees of freedom of the system, in order to improve accuracy. We have thus constrained the four coefficients A_{sp}, A_{sd}, A_{ds}, and A_{dp} in Eqs. (1) to remain equal to zero. As predicted, this reduced scatter on the remaining five statistically significant coefficients while introducing no detectable systematic bias.

IV. EXPERIMENTAL RESULTS

The rate coefficients appearing in Eqs. (1a), (1b), and (1c) include radiative and collisional contributions and are expected to have a linear dependence on neutral helium concentration [He] and on electron concentration [e]

$$A = \Gamma + k_{\mathrm{He}}[\mathrm{He}] + k_e[e]. \tag{2}$$

Γ is the radiative transition probability and k_{He} and k_e are two-body rate coefficients for deexcitation through neutral and electron collisions, respectively.

The five statistically significant coefficients, viz. the total deexcitation rates A_{ss}, A_{pp}, and A_{dd} of the He $3\,^3S$, $3\,^3P$, and $3\,^3D$ levels, and the excitation transfer rates A_{ps} [He($3\,^3P$) to He($3\,^3S$)] and A_{pd} [He($3\,^3P$) to He($3\,^3D$)] are shown on Fig. 3 as a function of electron density at a neutral density of 9.7×10^{17} cm^{-3} at 300 °K. The measured rate coefficients are seen to be essentially constant over the range 10^{11} to 3×10^{11} cm^{-3}, the influence of electron-induced excitation transfer becoming discernible at an electron density around 4×10^{11} cm^{-3}. Typical error bars result from the statistical analysis described in the preceding section; they are representative of the errors introduced through the analysis of each decay curve, and are of the same order as data reproducibility. They are much larger for the rate coefficients deduced from the $3\,^3D$-$2\,^3P$ transition at 5875 Å which has a much lower signal-to-noise ratio (see Fig. 2).

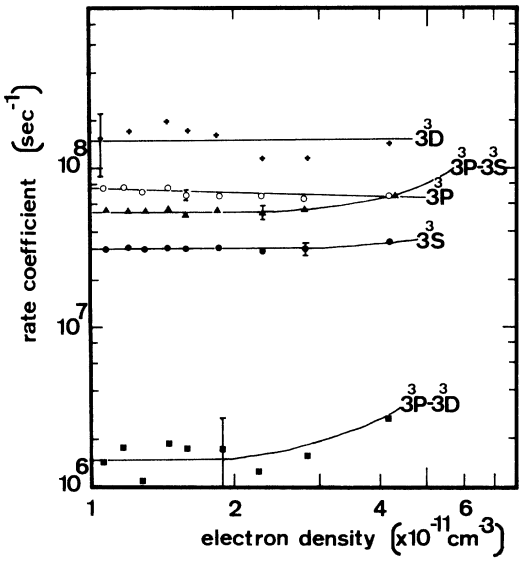

FIG. 3. Measured absolute value of rate coefficients as a function of electron density, for [He] = 9.7×10^{17} cm^{-3} and T_g = 300 °K. In the notation of Eqs. (1), triangles correspond to A_{ps}, dots to A_{ss}, crosses to A_{dd}, open circles to A_{pp}, and squares to A_{pd}. Solid lines are drawn as an aid to the eye and error bars result from the least-squares analysis described in Sec. III.

Similar results were obtained at lower neutral densities in the range $(2.6\text{–}9.7)\times10^{17}$ cm^{-3}, and it was always possible to obtain electron-density independent rate coefficients around $[e]\sim10^{11}$ cm^{-3} over this neutral density range. Measurements at lower neutral densities were not retained because the electrons were not thermalized during the pe-

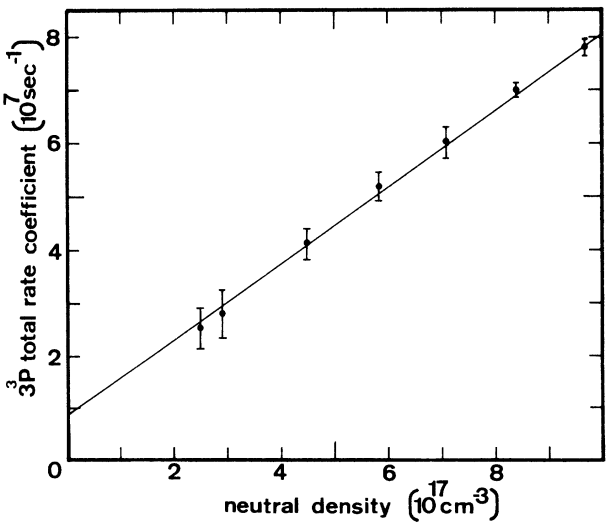

FIG. 4. Total deactivation rate coefficient of He($3\,^3P$) as a function of helium density at 300 °K; the solid line is the linear least-squares fit to the data.

TABLE I. Summary of radiative and collisional deactivation rates at 300 °K.

Level	Two-body collisional rate at 300 °K (10^{-11} cm^3 sec^{-1})	Radiative transition probability (10^6 sec^{-1}) Measured in this experiment	Accepted value [a]
$3\,^3S$	0.268 ± 0.01	29 ± 3	27.8
$3\,^3P$	7.14 ± 0.2	9.15 ± 2	9.48
$3\,^3D$	8.0 ± 1	60 ± 15	70.6
$3\,^3P$-$3\,^3D$	0.20 ± 0.05		
$3\,^3P$-$3\,^3S$	5.37 ± 0.5	< 2	1.08

[a] Reference 14.

riod over which measurements could be made. Whenever possible, the electron population was swept out of the afterglow cell with a microwave heating pulse, as described in Sec. II, to verify that the measured rate coefficients were indeed independent of electron density.

According to Eq. (2), the rate coefficients should fall on a straight line when plotted vs neutral density, with a slope proportional to the pressure-independent collisional rate constant k_{He} and with a zero-pressure intercept proportional to the radiative deexcitation rate Γ of the upper state of the observed transition. Typical results are shown on Fig. 4 for the $3\,^3P$-$2\,^3S$ transition. Error bars are statistical and represent one standard deviation around the average value of results similar to those shown on Fig. 3 at a particular neutral density, in the limit where they are independent of electron density. In the case of Fig. 4, the slope corresponds to a rate of two-body quenching by neutral collisions of 7.14×10^{-11} cm^3 sec^{-1} and the zero-pressure intercept to a radiative transition probability of 9.15×10^6 sec^{-1}.

Measured radiative and collisional deexcitation rates at 300 °K are summarized on Table I. Radiative transition probabilities compare well with accepted values.[14]

Similar measurements were made at various neutral temperatures over the range 300 to 600 °K. As indicated in Sec. II, the waveguide was then removed and replaced by a small oven to vary gas temperature; it was thus not possible to keep a close control on afterglow plasma parameters through microwave diagnostics. However, as electron density decreases monotonically with time in the afterglow while neutral density remains constant, the effect of electron collisions can be easily minimized by waiting long enough for the measured rates to become independent of time in the afterglow. This is in fact equivalent, with a change in horizontal scale, to the procedure used on Fig. 3 to identify rates independent of electron density, and it yields obviously the same results at 300 °K.

V. DISCUSSION

The thermally averaged cross sections $\bar{Q}$ are related to the rate constants k_{He} defined by our Eq. (2) by

$$k_{He} = \bar{Q}\bar{v}. \tag{3}$$

where $\bar{v} = (8kT/\pi M_r)^{1/2}$ is the average thermal velocity, M_r being the reduced mass of the collision partners (2 a.u. for ^{4}He).

The two nondiagonal excitation transfer rates A_{ps} and A_{pd} lead directly through Eq. (3) to thermally averaged experimental cross sections for excitation transfer $\bar{Q}_{tr}$ which may be directly compared to the values listed by Cohen in Table I of Ref. 2; they are shown on Fig. 5.

$\bar{Q}_{tr}$ ($3\,^3P$ to $3\,^3D$) is shown on Fig. 5(a). Our experimental points as well as the results of Wellenstein and Robertson[4] are markedly below the theoretical predictions of Cohen. The main contribution to this transfer in the low-energy range comes from the $3p$-$3d$ channel (a diabatic curve is denoted by the Rydberg electron) in the $^3\Pi_u$ symmetry, with a sharp threshold at 537 cm^{-1}. At higher energies, an additional $3p$-$3d$ contribution in the $^3\Sigma_u^+$ symmetry arises from tunnelling through the 0.3 eV barrier of the $3d$ state.[2]

The position of the threshold is beyond doubt for such an endothermic transition and the discrepancy can only arise from the absolute value of the cross section. The full line on Fig. 5(a) corresponds to the thermally averaged transfer cross section quoted by Cohen[2] while the dashed line was computed from the inverse process using detailed balance

$$\bar{Q}_{tr}(3\,^3P \to 3\,^3D) = \bar{Q}_{tr}(3\,^3D \to 3\,^3P)\frac{g_{3D}}{g_{3P}} \exp\left(\frac{E_{3P} - E_{3D}}{kT}\right), \tag{4}$$

with obvious notations. It is interesting to note that Cohen's results do not satisfy detailed balance despite his explicit use of microreversibility

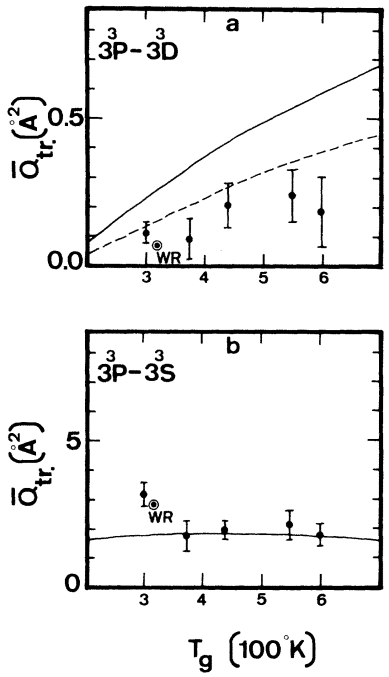

FIG. 5. Thermally averaged excitation transfer cross sections of He($3\,^3P$) as a function of neutral temperature (dots: this experiment; WR: Ref. 4). (a) $3\,^3P$-$3\,^3D$ transfer; solid line, theory of Cohen; dashed line, Eq. 4 of text. (b) $3\,^3P$-$3\,^3S$ transfer; solid line, theory of Cohen.

and that our experimental points are in much better agreement with the results of Eq. (4). We do not have any satisfactory explanation for this fact; detailed balance was verified by the experimental results of Wellenstein and Robertson.

Excitation transfer cross sections from the $3\,^3P$ to the $3\,^3S$ levels are shown on Fig. 5(b). While the overall agreement between theory and experiment is good at neutral temperatures above 400 °K, our experimental point at 300 °K as well as the result of Wellenstein and Robertson[4] at 320 °K are significantly above the theoretical curve. The only symmetry which contributes to the transfer cross section is $^3\Sigma_g^+$ with an almost zero threshold and a sharply rising edge at energies close to 10^{-2} eV. The $^3\Sigma_u^+$ symmetry gives no direct contribution to this process as the $3p$ diabatic molecular state undergoes no crossing with the $3s$ state. A possible explanation may conceivably lie in a slight overestimate of the potential barrier of the $3p$ state of $^3\Sigma_g^+$ symmetry,[3] but systematic or statistical uncertainties cannot be ruled out for this particular point, especially if one considers the fact that the total $3\,^3P$ deactivation cross sections are nearly equal at 300 and 380 °K (see Fig. 8 below).

Diagonal global deexcitation rates A_{ss}, A_{pp}, and A_{dd} are related to linear combinations of the individual cross sections tabulated by Cohen. Under our experimental conditions, deexcitation of a given level occurs mainly through the excitation transfer process

$$\mathrm{He}(n\,^3L) + \mathrm{He}(1\,^1S) \rightarrow \mathrm{He}(n'\,^3L') + \mathrm{He}(1\,^1S), \qquad (5)$$

and through associative ionization, often referred to as the Hornbeck-Molnar process

$$\mathrm{He}(n\,^3L) + \mathrm{He}(1\,^1S) \rightarrow \mathrm{He}_2^+(v,K) + e, \qquad (6)$$

where in our case $n=3$, $n'=2$, 3, or 4 and $L, L' = S$, P, or D. Direct measurement of the associative ionization rate is not possible with our experimental method.

The probability that an atom initially on any $3\,^3L$ level may be transferred onto any $4\,^3L'$ level by collision with a ground-state thermal atom is negligibly small, the threshold energy being of order 1 eV. Transfers between singlet and triplet states are negligible under the present experimental conditions, as determined by monitoring the lines originating from $3\,^1L$ states. However, exothermic collisions from $3\,^3L$ states to either $2\,^3S$ or $2\,^3P$ states are possible and the corresponding cross section may *a priori* be large.[2,3]

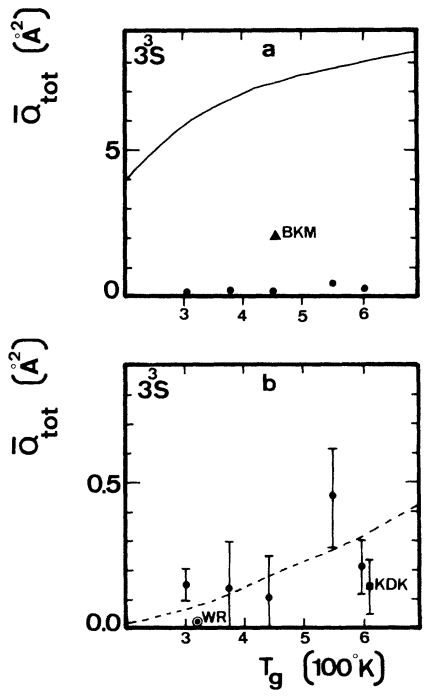

FIG. 6. Total deactivation cross section of He($3\,^3S$) as a function of neutral temperature; dots are present experiment and BKM, KDK, and WR correspond, respectively to Refs. 15, 16, and 4. See text for discussion. (a) Solid line: addition of $\bar{Q}_i$ and $\bar{Q}_{tr}$ tabulated by Cohen; (b) dashed line: $\bar{Q}_i$ tabulated by Cohen.

The diagonal global deexcitation rate is related through Eqs. (2) and (3) to the total averaged cross section $\bar{Q}_{tot}$ for destruction of any $3\,^3L$ level. It is the sum of the cross sections for the individual processes:

$$\bar{Q}_{tot}(3\,^3L) = \bar{Q}_i(3\,^3L) + \sum_{L' \neq L} \{\bar{Q}_{tr}(3\,^3L \rightarrow 3\,^3L') + \bar{Q}_{tr}(3\,^3L \rightarrow 2\,^3L')\}. \quad (7)$$

The individual theoretical cross sections $\bar{Q}_i$ and $\bar{Q}_{tr}$ are given in Table I of Ref. 2.

The total deexcitation cross section for the $3\,^3S$ level is shown on Fig. 6. It was already noted in Sec. III that the transfer rates of $He(3\,^3S)$ to $3\,^3P$ or $3\,^3D$ are negligible at thermal energies because of the small Boltzmann factor. The only two significant deactivation channels which remain open to this state are associative ionization to form molecular ions and an exothermic transition to the $2\,^3P$ state.

The solid line in Fig. 6(a) corresponds to the sum of these two processes according to the predictions of Cohen, as a function of gas temperature. Experimental results are considerably below theoretical predictions (the points labelled BKM, WR, and KDK correspond to measurements by Bennet, Kindlemann, and Mercer,[15] by Wellenstein and Robertson,[4] and by Kubota, Davies, and King[16]). However, if we assume that $\bar{Q}_{tr}(3\,^3S \rightarrow 2\,^3P) = 0$, agreement becomes quite good in absolute value and in temperature dependence between our experimental results and the thermally averaged cross sections for associative ionization $\bar{Q}_i(3\,^3S)$ computed by Cohen. This can be understood by noting that in the diabatic states model for scattering, the main contribution to the $3\,^3S$-$2\,^3P$ excitation transfer cross section is through a curve crossing[1] around 4 a.u. between the $3s$ attractive diabatic potential and the $2p$ repulsive potential of $^3\Sigma_u^+$ symmetry. Small potential barriers occur in most of the diabatic states of Σ symmetry; this explains why the cross section has a nonzero threshold for $3\,^3S$-$2\,^3P$ transfer. The present experimental results strongly suggest that the height of the potential barrier which was previously estimated to be of the order of 1.1×10^{-2} eV at a distance of 10 a.u. is undervalued in the existing calculations. Moreover, the strength of the radial coupling near the above-mentioned curve crossing may be overestimated. Further theoretical studies would be extremely useful.

Figures 7 and 8 show the results for the total deexcitation cross sections of the $3\,^3D$ and $3\,^3P$ states. Again, the theoretical individual components of the total cross sections tabulated by Cohen are shown together with the present experimental

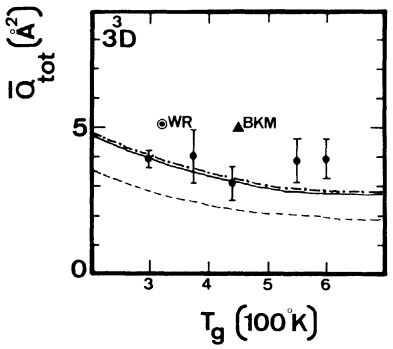

FIG. 7. Total deactivation cross section of $He(3\,^3D)$; dots are present experiment, and BKM and WR correspond, respectively, to Refs. 15 and 4. The lines are predictions of Cohen's theory: dash-dotted line, total cross section; full line, same neglecting $n = 3$ to $n = 2$ transfer; dashed line, associative ionization cross section.

results and with former measurements.[4,15] Bridgett *et al.*[17] have reported maximum values of these cross sections of 2×10^{-16} and 1×10^{-16} cm^2, respectively, without indicating neutral gas temperature. Overall agreement is good between theory and experiment, but some points are worth discussing.

In Fig. 7, the dash-dotted line corresponds to the total theoretical cross section, while the full line corresponds to setting $\bar{Q}_{tr}$ $(3\,^3D$-$2\,^3P) = 0$ and retaining only associative ionization and collisional transfer between $n = 3$ states. In this case, the strongly exothermic collisional transition between $n = 3$ and $n = 2$ triplet states appear to be negligible both theoretically and experimentally.

If we turn now to Fig. 8, we note that while theory predicts a small contribution of the $n = 3$ to $n = 2$ transfer, this does not seem to be substantiated

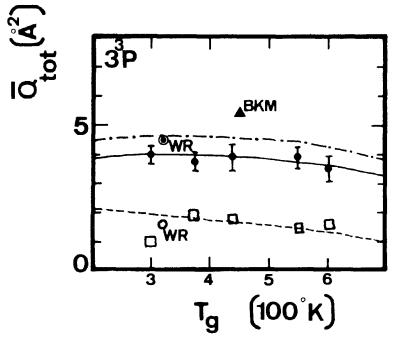

FIG. 8. Total deexcitation cross section of $He(3\,^3P)$; same comments as for Fig. 7. The open squares correspond to the experimental associative ionization cross section obtained by subtracting the transfer cross sections to $3\,^3D$ and $3\,^3S$ [Fig. 5(a) and 5(b)] from the total deactivation cross section.

experimentally either. Subtraction of the experimental transfer cross sections to $3\,^3S$ and $3\,^3D$ from the experimental total deactivation cross section of $He(3\,^3P)$ results in the open squares; they are in good agreement, except at 300 °K, with the theoretically predicted cross section for associative ionization (dashed line).

VI. CONCLUSIONS

The present work complements the theoretical study of Cohen[1,2] in that experimental determination of cross-section values and of their temperature dependence bring complementary and useful information on the intermolecular potentials and coupling between states. The multistate curve-crossing model appears to be remarkably successful in describing associative ionization and excitation transfer by collision with neutral atoms among the $n = 3$ terms of the helium triplet system. Its description of collisional transfer between $n = 3$ and $n = 2$ states, on the other hand, is unsatisfactory — particularly for He $3\,^3S \rightarrow 2\,^3P$ transfer; the $^3\Sigma_u^+$ scattering contribution is apparently considerably overestimated, either because of small errors in the computed potential curves, or because of incorrect estimates of the coupling matrix elements.

The techniques of time-resolved laser fluorescence spectroscopy are particularly promising for studies of excitation transfer in thermal collisions, from cryogenic temperatures (below 4.2 °K in helium) to elevated temperatures well above 1000 °K. They can be readily applied to many other atomic and molecular systems, where most excited states of interest can be reached either from the ground state or from a long-lived excited state, under closely controlled conditions in a low-power, stationary afterglow.

[1]J. S. Cohen, Phys. Rev. A 13, 86 (1976).
[2]J. S. Cohen, Phys. Rev. A 13, 99 (1976).
[3]W. J. Steets and N. F. Lane, Phys. Rev. A 11, 1994 (1975).
[4]H. F. Wellenstein, and W. W. Robertson, J. Chem. Phys. 56, 1072 (1972); 56, 1077 (1972); 56, 1411 (1972).
[5]R. M. Measures, J. Appl. Phys. 39, 5232 (1968).
[6]C. B. Collins, B. W. Johnson, and M. J. Shaw, J. Chem. Phys. 57, 5310 (1972).
[7]J.-C. Gauthier, J.-P. Geindre, J.-P. Moy, and J.-F. Delpech, Phys. Rev. A 13, 1781 (1976).
[8]J.-P. Moy, J.-C. Gauthier, and J.-P. Geindre, in Proceedings of the Twelfth International Conference on Phenomena in Ionized Gases, Eindhoven, 1975, p. 16 (unpublished).
[9]J.-F. Delpech, J. Boulmer, and J. Stevefelt, in *Advances in Electronics and Electron Physics*, edited by L. Marton (Academic, New York, 1975), Vol. 39, p. 121.
[10]J. Boulmer, F. Devos, J. Stevefelt, and J.-F. Delpech, to be published.
[11]J.-F. Delpech and J.-C. Gauthier, Phys. Rev. A 6, 1932 (1972).
[12]J.-P. Moy, thesis (Orsay, 1976) (unpublished).
[13]E. D. Cehelnik, K. D. Mielenz, and R. A. Velapoldi, J. Res. Natl. Bur. Stand. 79A, 1 (1975).
[14]W. L. Wiese, M. W. Smith, and B. M. Glennon, *Atomic Transition Probabilities*, NSRDS-NBS 4 (U.S. GPO, Washington, D. C., 1966) Vol. 1.
[15]W. R. Bennett, Jr., P. J. Kindlmann, and G. N. Mercer, Appl. Opt. Suppl. 2, 34 (1965).
[16]S. Kubota, C. Davies, and T. A. King, J. Phys. B 8, 1220 (1975).
[17]K. A. Bridgett, T. A. King, and R. J. Smith-Saville, J. Phys. E 3, 767 (1970).